Ocean Engineering 171 (2019) 25–32

Contents lists available at ScienceDirect

Ocean Engineering

journal homepage: www.elsevier.com/locate/oceaneng

Experimental investigation on hydrodynamic performance of a breakwater-integrated WEC system

X.L. Zhao[a], D.Z. Ning[a,*], D.F. Liang[b]

[a] State Key Laboratory of Coastal and Offshore Engineering, Dalian University of Technology, Dalian, 116024, China
[b] Department of Engineering, University of Cambridge, Cambridge, CB2 1PZ, UK

ARTICLE INFO

Keywords:
Wave energy converter
Breakwater
Heave response amplitude
Transmission coefficient
Wave force

ABSTRACT

An integrated breakwater-WEC system, which comprises of an array of heaving Oscillating Buoy Wave Energy Converters (OB-WECs) attached at the weather side of a fixed breakwater, is proposed in this study. Detailed experiments have been undertaken to investigate the heave-response-amplitude operator (HRAO), the wave force on the WEC devices and the transmission coefficient of the breakwater-WEC system. The design of the experiment is validated by comparing the HRAO of the devices with the corresponding numerical results. The hydrodynamic performance of the breakwater-WEC system is compared with that of its isolated counterparts, i.e., the isolated WEC array and the isolated breakwater. Parametric studies are conducted to optimise the draft of the WEC devices and the breakwater-WEC spacing, i.e. the gap between the WEC devices and the breakwater. Results show that, compared with the case of isolated WEC devices, the wave force and HRAO of the WEC devices are amplified for a properly designed breakwater-WEC system. Even though the external damping (caused by viscous damping and the friction loss) plays an important role while evaluating the efficiency of the WECs, the existence of the breakwater significantly improves the performance of the WEC array. The HRAO is sensitive to the draft of the devices and breakwater-WEC spacing.

1. Introduction

As one of the marine renewable energy resources, wave energy is attractive for its vast reserve (Pecher and Kofoed, 2017). However, the high construction-cost limits the industrialization of wave energy exploitation. The cost-sharing of the infrastructures built for different purposes is a promising idea to reduce the cost of marine renewable energy development by combining wave energy devices with other coastal or offshore structures. Recently, many hybrid-structures have emerged, such as WEC-offshore wind turbine integrations (Karimirad, 2014), WEC-breakwater integrations (Mustapa et al., 2017), WEC-offshore platform integrations, etc. Advantages of these hybrid systems include infrastructure-sharing, space-sharing and multi-purpose. This integration strategy can greatly enhance the economic competitiveness of wave energy utilization.

Breakwaters are widely-used in coastal and offshore engineering (McCartney, 1985). The breakwaters and the wave energy converters are often deployed in similar marine environmental conditions, and they also share some similarities in the structural design. Based on these similarities, many breakwater-WEC systems have been proposed, such as the caisson breakwater-Oscillating Water Column (OWC) type (Boccotti, 2007), the sloping breakwater-overtopping type (Contestabile et al., 2017), pile-restrained floating breakwater-the Oscillating Buoy (OB) type (Ning et al., 2016). Breakwaters with rectangular-section, which is commonly termed as the pontoon-type breakwater, are frequently deployed with the advantages of simplicity and durability (Hales, 1981). It is understood that the wave conditions at the weather side of the pontoon-type breakwater can be regarded as the superposition of the incident and reflected waves (Drimer et al., 1992). Hence, improvement to the power generation efficiency is expected by placing wave energy converters on the weather side of the breakwater. There have been some studies aiming at improving the energy conversion efficiency by exploiting the reflective energy from the sea wall or the pontoon. Howe and Nader (2017) experimentally investigated the performance of OWC WEC in front of a bottom-mounted breakwater. McIver and Evans (1988), Mavrakos et al. (2004) and Schay et al. (2013) investigated the point absorbers in front of a sea wall. Zhao et al. (2017) and Ning et al. (2018) investigated the performance of the OB-WEC in front of a fixed pontoon based on linear potential flow theory. Results show significant increase of the power extraction by the WECs with the presence of a downstream wall. All of the studies show that the superposition of the incident wave and reflected wave

* Corresponding author.
E-mail address: dzning@dlut.edu.cn (D.Z. Ning).

https://doi.org/10.1016/j.oceaneng.2018.10.036
Received 7 March 2018; Received in revised form 5 September 2018; Accepted 23 October 2018

improves the efficiency of the WECs located on the weather side of a seawall or a pontoon.

As a common wave energy device, OB-WEC has been proved to be an effective way for wave energy extraction (Falnes and Hals, 2012; Rahmati and Aggidis, 2016; Tampier and Grueter, 2017). In the present study, a system comprising of an array of OB-WECs located at the weather side of the pontoon-type breakwater is studied systematically. The hydrodynamic performance of the OB-WECs has already been investigated extensively. To the authors' knowledge, these pioneering studies rarely consider the effect of the adjacent structures on the performance of the WECs, especially from point view of the physical model test. The present study aims to explore the effect of the adjacent structures on the WECs by the physical model test and the extended numerical calculation.

The methods used in the field of wave interaction with WECs include theoretical method, numerical method and experimental method. Theoretical investigations are often conducted based on linear potential flow theory using matching eigenfunction function method, which is suitable for the bodies with regular shape (Göteman, 2017). Numerical methods are generally divided into two categories: frequency domain and time domain. For the former category, the Boundary Element Method (BEM) based on potential flow theory is often used and successful studies with focus on the preliminary investigations have been achieved (Bellew, 2011). The latter category mainly includes the method based on Cummins' decomposition with premise of the frequency domain calculations (Babarit and Clément, 2006) and the wave flume (or tank) technique based on fully nonlinear potential flow theory or Computational Fluid Dynamics (CFD) method (Chen et al., 2017). In this paper, we combine the experimental method and numerical predictions in frequency domain. The experimental measurement of the hydrodynamic properties of the system is performed firstly. Then extended numerical calculations are conducted by considering the viscous damping and friction damping derived from the experiments.

For the breakwater-WEC system, both the energy conversion efficiency and the transmission coefficient are of interest to the practical application. The heave response amplitude of a heaving OB-WEC can be used to indicate the potential for power generation. In this paper, the heave response amplitude, the wave force on the WEC devices and the transmission coefficient of the breakwater system are investigated experimentally. The effects of the draft of the WEC devices and the spacing between the pontoon and the WEC devices, i.e. pontoon-WEC spacing, are examined. Extended numerical predictions on the power-take off (PTO) performance of the WEC array are performed by considering the external damping (caused by viscous damping and friction loss), which can be obtained from physical model tests. Influence of the breakwater on the PTO performance of the WEC array is illustrated. The paper is structured as follows. Section 2 describes the experimental setup and test procedures. Section 3 presents the results for parametric study, extended numerical calculation and discussions. Finally, the conclusions are given.

2. Laboratory experiments

The experiments are conducted in a wave flume at the State Key Laboratory of Coastal and Offshore Engineering, Dalian University of Technology, China. The dimensions of the flume are 69 m in length, 2 m in width and 1.8 m in depth. A piston-type unidirectional wave-maker is installed at one end of the flume, and a wave-absorbing beach is located at the other end to reduce the wave reflection.

Fig. 1 shows the layout of the physical model, which consists of the WEC devices and the breakwater. Four identical WEC devices with radius of $a = 0.135$ m are equally spaced on the weather side of the breakwater. The spacing between two neighbouring devices is $s_2 = 0.5$ m. The width (in the wave-propagation direction) and the transverse length (along the wave-crest direction) of the breakwater is $B = 0.6$ m and $D = 1.99$ m, respectively. In order to avoid possible collisions while installing the breakwater model, a 0.5 cm gap is left between each side of the breakwater and the flume wall. Each WEC device is guided by two slide rails and moves only in the heave mode, whereas the rear breakwater is fixed. The dimensions of the cross-section of the slide rail is 0.04 m×0.03 m, which is sufficiently small so that the influence of the slide rail on wave field can be neglected. Fig. 2 shows a sketch of the experimental setup. Two wave gauges are placed on the lee side of the breakwater to record the water surface elevations. The distance between the two wave gauges is 0.5 m. The cases of the breakwater without WEC devices, hereinafter referred to as the isolated breakwater, and the WEC devices without the breakwater, hereinafter referred to as the isolated WEC devices, are also considered in the experiments for comparison purposes.

Fig. 1. Physical model of the WECs and the breakwater, with the WECs numbered as device #1–4 respectively.

In the experiments, the still water depth is fixed at $h = 1$ m and the draft of the rear breakwater is configured to be $d_0 = 0.25$ m. The tested wave conditions are summarized in Table 1, while the structural layout parameters are summarized in Table 2. To ensure the accuracy of experiments, each test case is repeated twice.

The data acquisition system mainly includes the wave height recording system, the displacement measuring system and the force balance system. The wave height acquisition system includes wave gauges and the associated data processing system. The measuring range of the wave gauges is 60 cm, with the maximum error of 0.01 cm. The displacement measurement system includes the displacement sensor and the data processing system. The measuring range of the displacement sensor is 60 cm, with the maximum error of 0.06 cm. The force balance system is used to measure the wave force on the WEC devices. The measuring range of the force balance system is 300 N, and the maximum error is 1.5 N. According to the data measured by two wave gauges, the transmitted wave amplitude (A_T) can be obtained. The transmission coefficient is then calculated to be $K_T = A_T/A$. The heave response amplitude ζ can be obtained from the heave response measured by the displacement measurement system. The heave-response-amplitude operator (HRAO) ξ is then calculated to be $\xi = \zeta/A$.

3. Results and discussions

3.1. Comparison of the experimental and numerical results

Firstly, a free decay test is conducted to determine the natural frequency and the external damping (caused by the viscous loss and friction loss) of the WEC device. An isolated WEC device is placed at the centre of the wave flume in the free decay test. Fig. 3 plots the time history of the heave response of the WEC device (draft $d = 0.2$ m). Based on this response, the natural period T_{nat} of the WEC device can be determined to be 1.06 s, which agrees well with the result predicted using linear potential flow theory. Correspondingly, the natural frequency ω_0 is 5.91 rad/s. The dimensionless damping coefficient can be

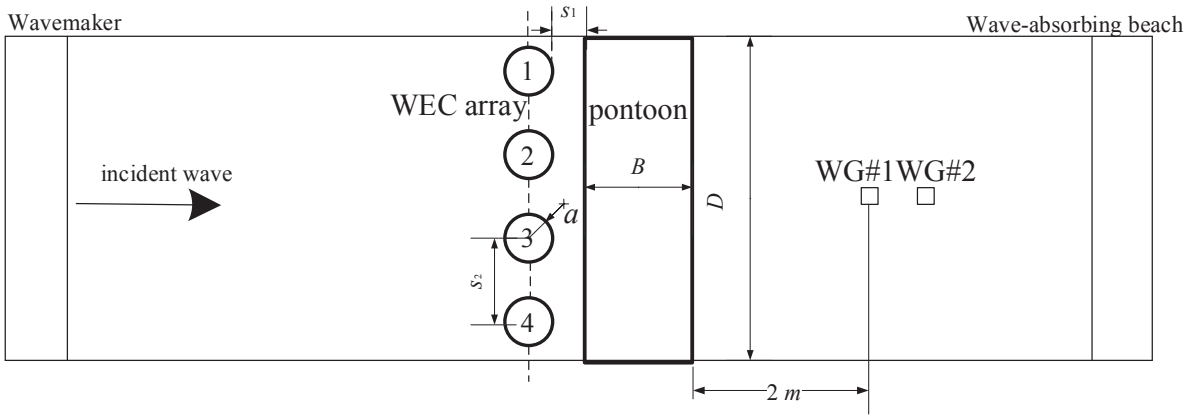

Fig. 2. Sketch of the experimental setup for the breakwater-WEC system (the wave gauges are numbered as WG #1–2).

Table 1
Wave conditions, with T denoting the wave period, A the incident wave amplitude and kh the dimensionless wave number.

T (s)	1.1	1.17	1.22	1.27	1.33	1.4	1.5	1.6	1.7	1.8	1.9
A (m)	0.06	0.06	0.06	0.06	0.06	0.06	0.06	0.06	0.06	0.06	0.06
Kh	3.334	2.954	2.726	2.526	2.318	2.112	1.874	1.684	1.528	1.402	1.306

Table 2
Structural parameters, with d denoting the draft of the WEC devices, s_1 the pontoon-WEC spacing.

	d (m)	a (m)	s_1 (m)	d_0(m)	B (m)
Case1	0.20	0.135	0.05	0.25	0.6
Case2	0.20	0.135	0.10	0.25	0.6
Case3	0.20	0.135	0.20	0.25	0.6
Case4	0.15	0.135	0.10	0.25	0.6
Case5	0.10	0.135	0.10	0.25	0.6
Case6	0.20	0.135	–	–	–
Case7	–	–	–	0.25	0.6

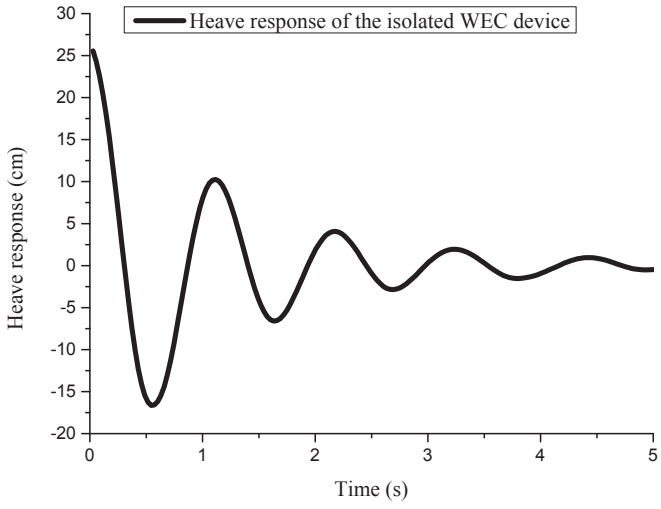

Fig. 3. Time history of the heave response of the WEC device in the free decay test.

determined by using the formulae of $\varkappa = \frac{1}{2\pi}\ln(\frac{z_i - z_{i-1}}{z_{i-2} - z_{i-3}})$, where z_i are the successive peak or trough values of the heave response in the free decay test. The external damping b_{ext} can be obtained by using $b_{ext} = \frac{2\varkappa\rho g S}{\omega_0} - \lambda(\omega_0)$, where $\lambda(\omega_0)$ ρ, g and S denote radiation damping, water density, gravitational acceleration and waterline area of the buoy, respectively (Journée and Massie, 2001). The radiation damping

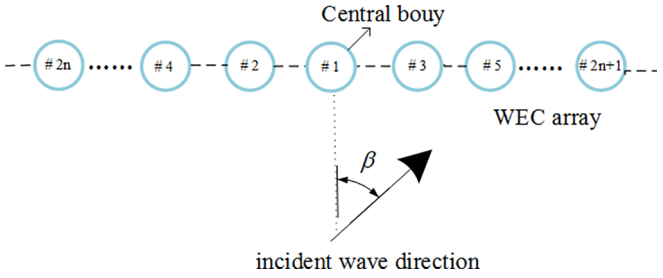

Fig. 4. The sketch of the layout the of WEC array in the numerical calculation.

$\lambda(\omega_0)$ is calculated by using the Higher Order Boundary Element Method (HOBEM) package WAFDUT, which is developed based on linear potential flow theory (Teng and Taylor, 1995). The waterline area S is calculated as πa^2. For the present cylinder, the dimensionless damping coefficient and external damping are $\varkappa = 0.141$ and $b_{ext} = 23.4$ kg/s.

Theoretically, the hydrodynamic properties of a structure in a channel can be predicted by considering a structure (at the central location) in an infinite array consisting of identical equally spaced structures. Since the effect of the devices far away from the targeted devices is quite small on the targeted devices, the problems can be simplified as the hydrodynamics of an array with finite buoys. Similar application can be seen in Ref. (Gomes et al., 2016). In this study, an array consisting of 31 equally-spaced cylinders (with draft of 0.2 m, radius of 0.135 m, WEC-WEC distance of 0.50 m) is investigated numerically based on linear potential flow theory in frequency domain. The layout of the WEC array is shown in Fig. 4. Considering the external damping b_{ext}, the motion equation in heave mode of the targeted device (i.e., the central device of the array) is written as:

$$(-\omega^2(\mathrm{M}+\mu) - \mathrm{i}\omega(b_{ext} + \lambda + \lambda_{PTO}) + K)A_R = F_z \quad (1)$$

where ω is the angular wave frequency, i the imaginary unit, M and K are the mass and buoyance stiffness of the central body, which is calculated as $\rho\pi a^2 d$ and $\rho g\pi a^2$, respectively. The added mass and radiation damping in Eq. (1) can be expressed as $\mu = \sum_{j=1}^{N}\mu_1^j$ and $\lambda = \sum_{j=1}^{N}\lambda_1^j$, where μ_i^j and λ_i^j are the added mass and damping coefficient of the ith body (i.e., device #i) in heave mode due to the heave motion of the jth device, respectively (i, j = 1, 2, …N). λ_{PTO} denotes the PTO damping

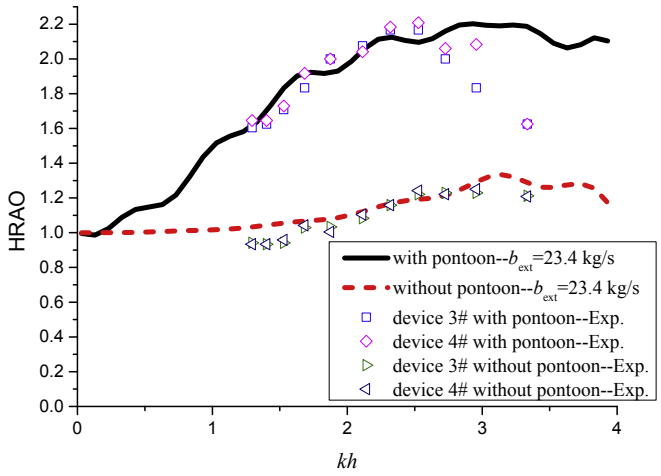

Fig. 5. Comparison of the HRAO between the numerical and experimental results.

acting on the device. A_R and F_z are the heave response amplitude and wave exciting force in heave mode of the nth device, respectively. The HRAO of a device can be expressed as $A_{R,n}/A$. N is the total number of the WECs in the array. The hydrodynamic calculations are conducted by using WAFDUT. The incident wave angle is chosen as $\beta = 0^\circ$ in the present numerical calculation.

In the context of comparisons, the HRAO corresponding to the targeted device is chosen to compare with the corresponding experimental results (i.e., HRAO of device #3 and #4 in Fig. 2). To form the breakwater-WEC integrated system, a pontoon (with length of 20 m, draft of 0.25 m, and breadth of 0.6 m) was arranged at the lee side of the cylinder array. For the case of WEC array without the breakwater, the pontoon is removed from the wave flume. In this sub-section, the PTO damping λ_{PTO} is set as zero. The external damping b_{ext} is considered as 23.4 kg/s. The other parameters in the numerical calculation are in accordance with those in the experiment.

Fig. 5 shows the comparisons between the numerical and experimental results for the devices with and without the pontoon. In the lower frequency range ($1.3 < kh < 2.8$), good agreement between the two sets of results can be found. However, discrepancies between the experimental data and numerical predictions can be found in the higher frequency range ($2.8 < kh < 3.3$), especially for the devices with the pontoon. This may be due to the fact that the wave nonlinearity at the weather side of the pontoon is strong and the numerical results are predicated using linear tool. Besides, the numerical calculations in frequency domain represent a large array of devices. Comparatively, only four devices are considered in the experiments. Number of interactions between different devices is limited for the experiment approach, and the interactions were fully considered under the context of linear potential flow theory. This may be one of the reasons that lead to the discrepancies between the two aspects. Overall, the two sets of results are in good agreement, which may verify the experiment.

3.2. Effect of the pontoon-WEC spacing (s_1)

One emphasis of the present work is to compare the hydrodynamic performance of the breakwater-WEC system with those in the corresponding isolated situations (i.e., the isolated breakwater and the isolated WEC devices). The HRAO of the WEC devices and the transmission coefficient of the breakwater are the main parameters used in this study to indicate the hydrodynamic performance of the integrated system. In this section, the effect of the pontoon-WEC spacing is examined by setting s_1 at 0.05 m, 0.10 m and 0.20 m respectively (see Cases 1–3 in Table 2).

Firstly, the repeatability of the experiment was checked by comparing the time histories of the heave response of the targeted devices for the two repeated tests. Note that, since the WECs are arranged symmetrically, only the results rresponding to the WEC devices (device #3 and #4) located on the right side are presented. Fig. 6 shows the time histories of the heave response corresponding to the case of $T = 1.27$ s and $A = 0.06$ m. It can be found that the experiment was repeated very well.

Fig. 7 shows the time histories and the amplitude spectra of the heave response of the WEC devices with the presence of the breakwater. It can be seen that the devices move with the same phase. From the amplitude spectra of the heave response of the devices, it can be concluded that the peak frequencies of the two devices are the same and the contribution from the second-order sum-frequency component is negligible. In addition, it can be seen that the shape corresponding to device #3 is wider than that corresponding to device #4. It is worth noting that, since the present problem represents an infinite long array of WECs, the HRAO and the corresponding amplitude spectra of device 3# and 4# shall be the same for the experimental results. However, there exist small discrepancies for some cases. This may be attributed to the fact that the external damping of each devices and wave field at different locations in the tank may be not the same completely. Of course, the instruments error within certain limits may also exist. These may lead to the small differences between the hydrodynamic properties of the two devices in this experiment.

Fig. 8 shows the HRAO (ξ) and transmission coefficient (K_T) as functions of the dimensionless wavenumber kh. From Fig. 8(a), it can be seen that there exists a small difference between the HRAO values for the device #3 and #4. Overall, the variations of HRAO with kh for device #3 and #4 are quite similar. Fig. 9 shows the time histories of

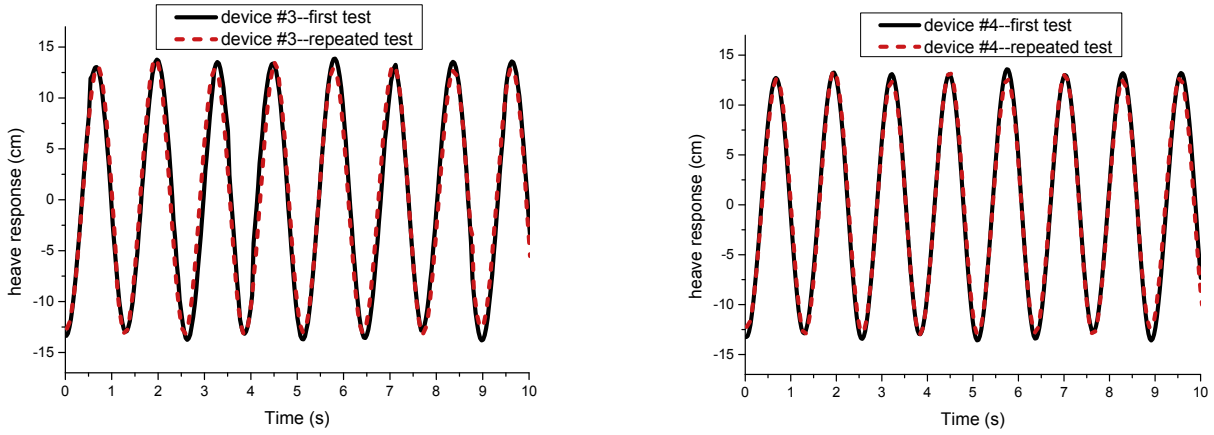

Fig. 6. Time histories of the heave response of the device 3# and 4# with the presence of the pontoon ($T = 1.27$ s, $A = 0.06$ m, $d = 0.20$ m, $s_1 = 0.05$ m).

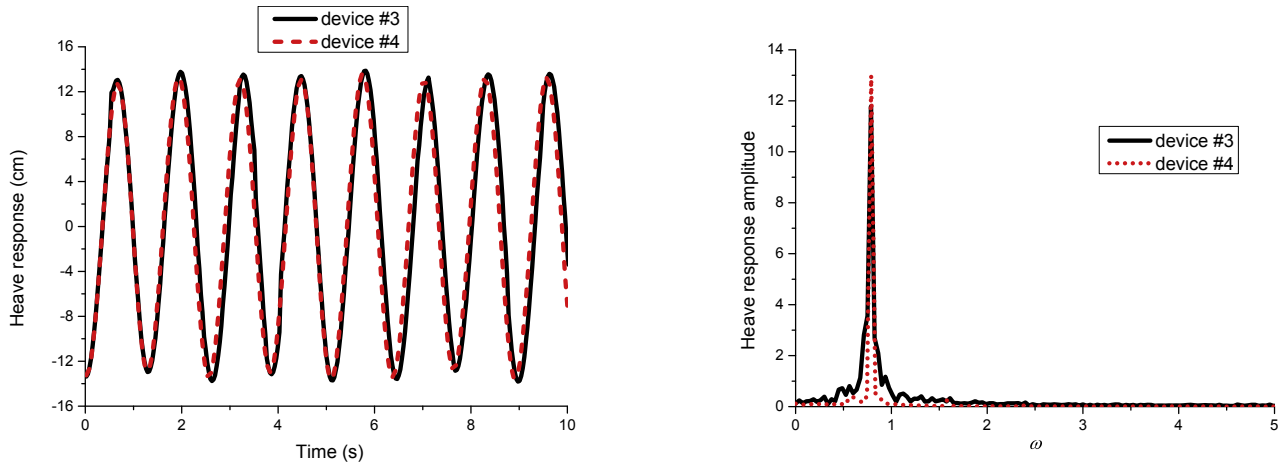

Fig. 7. Time histories (left) and the amplitude spectra (right) of heave response of the WEC devices (device #3 and #4) with the presence of the breakwater (T = 1.27 s, A = 0.06 m, d = 0.20 m, s_1 = 0.05 m).

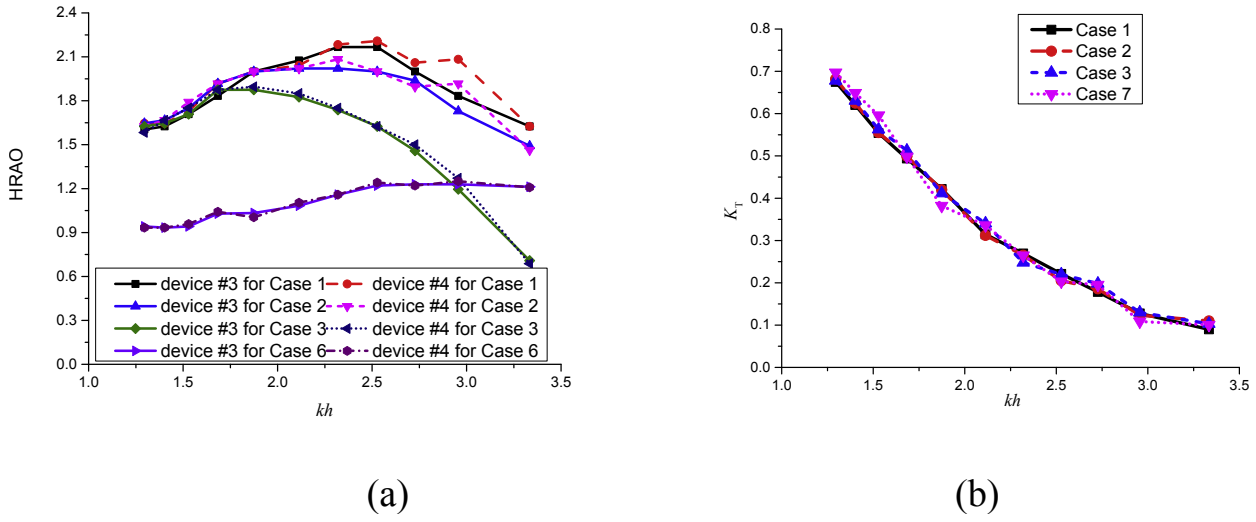

Fig. 8. Variations of the HRAO (a) and transmission coefficient (b) with the dimensionless wavenumber.

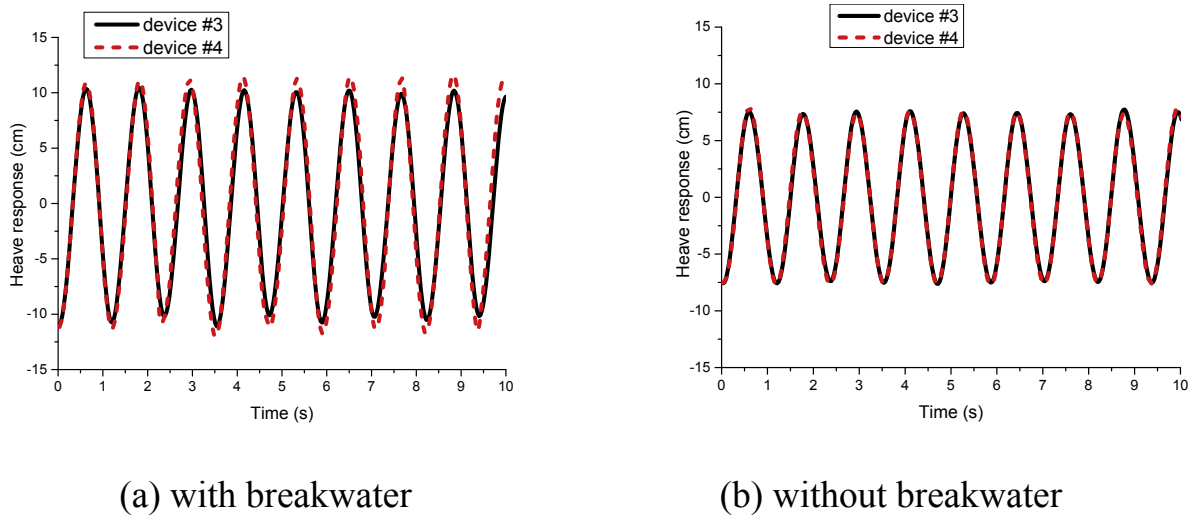

Fig. 9. Time histories of the heave response of the WEC devices (device #3 and device #4) for cases with and without the breakwater (T = 1.17 s, A = 0.06 m, d = 0.20 m, s_1 = 0.05 m).

the corresponding devices. Particularly, for the HRAO of devices with breakwater at kh = 2.954, the HRAO of the device at the outer sider is slightly greater than that at the inner side. However, this difference is absent for devices without breakwater. In spite of this, the main trends of the HRAO against kh are captured. The pontoon-WEC spacing has little effect on the HRAO of the WEC devices at the low frequency range

(1.3 < *kh* < 1.7 approximately). However, significant influence can be found at the high frequency range (1.7 < *kh* < 3.3), and the level of influence continually increases with the frequency. With regard to the tested pontoon-WEC spacings, the HRAO decreases with the increasing pontoon-WEC spacing. For the isolated WEC devices without the breakwater, HRAO observes consistently slight increase with the increasing *kh*. By comparing the HRAO variations of the WEC devices with and without the presence of the breakwater, it can be concluded that the presence of the breakwater amplifies the HRAO as long as the pontoon-WEC spacing is kept reasonably small. For the heaving OB-WECs, the HRAO value roughly indicates the potential for power generation. Hence, the energy conversion performance of the WECs with the breakwater is superior to that without the breakwater. It is understood that the superposition of the incident waves and the reflected waves is formed at the weather side of the breakwater, which directly amplifies the wave amplitude. For the waves formed at the weather side, there exists the quasi node and quasi anti-node at some locations. For devices located at the quasi node, the HRAO of the devices will be amplified significantly. In addition, the response of the devices will be mitigated while the devices located at the quasi anti-node. That is why the HRAO of the devices with breakwater is greater than that without breakwater and the reverse trend can be found for some cases (such as case 3 in Fig. 8(a)). This can also be used to explain the phenomena that the forces acted on the devices with breakwater is greater than that without the breakwater (as is shown in Fig. 13).

Fig. 8(b) shows the results of the transmission coefficient. It can be found that the pontoon-WEC spacing has little influence on the transmission coefficient in the tested frequency range. Moreover, the transmission coefficients of the breakwater with and without the presence of the WEC devices are nearly the same. Therefore, the wave attenuation performance of the original breakwater is not compromised by arranging the WECs on its weather side. Note that the PTO damping is not considered in the experimental study.

3.3. Effect of the draft of the WEC devices (d)

The effect of the draft of the WEC devices are investigated by considering $d = 0.05$ m, 0.10 m and 0.20 m, respectively (see Cases 2, 4 and 5 in Table 2). From Fig. 10(a), it can be seen that trend of the variations of HRAO with *kh* are all similar, which can be characterized as increasing firstly and then decreasing. The HRAO of the WEC device on the outer side is greater than that on the inner side at the high frequency range. Overall, the HRAO of the WEC devices increases with the increasing draft. From the variations of transmission coefficient with *kh* as shown in Fig. 10(b), it can be concluded that the draft of the WEC devices hardly affect the transmission coefficient of the breakwater system.

3.4. Wave forces on WEC devices

The results concerning the wave forces in heave mode are presented and discussed in this section. Fig. 11 shows the time histories of the heaving wave force on the WEC devices (device #3 and device #4) for case of $T = 1.27$ s, $A = 0.06$ m, $d = 0.20$ m and $s_1 = 0.05$ m, from which it can be seen that the wave forces on the two devices are the same phase. The presented wave force is non-dimensionalized by $\rho g \pi A a^2$. From the corresponding spectrum analysis of the wave forces in Fig. 12, it can be found that the contribution from the second-order component on the wave force is significant. The third-order and fourth-order components also arise, although their amplitude is not comparable to the first-order and second-order components. Fig. 13 show the variations of the $F_{max}/\rho g \pi A a^2$ on WEC devices #3 and #4 as the function of dimensionless wavenumber. Here, F_{max} denotes the maximum value of the measured wave force for a wave condition, which can be calculated as the averaged value of the maximums occurred in the time-histories (such as Fig. 11). It can be seen that, for both the cases with and without the pontoon, F_{max} on the WEC device located on the outer side is greater than that on the inner side. For the cases without the pontoon, F_{max} on the WEC device decreases with increasing *kh*. Comparatively, for the WEC devices with the pontoon, the curves of F_{max} *vs* *kh* also show a decreasing trend. At each tested wave frequency, the presence of the pontoon increases the F_{max} on devices #3 and #4. From the case of $T = 1.27$ s (see Fig. 12), it can be seen that the wave forces is characterized by the presence of the second-order component. By comparison, the second-order composition is absent for the heave response (see Fig. 7). This may be attributed to that the viscous effect and the friction effect (caused by relative motion of the device and the piles) eliminate the second-order component in heave response.

3.5. Extended predictions of performance of the WEC in a channel

Since the physical PTO system is not used in the experiments, extended numerical predictions on the PTO performance of the WEC are conducted based on linear potential flow. In this section, the external damping ($b_{ext} = 23.4$ kg/s) is considered while predicting the performance of the WEC. A WEC array consisting of 31 wave energy devices is used to calculate the hydrodynamics of the targeted devices. For case of the breakwater-WEC integrated system, a pontoon was arranged at the

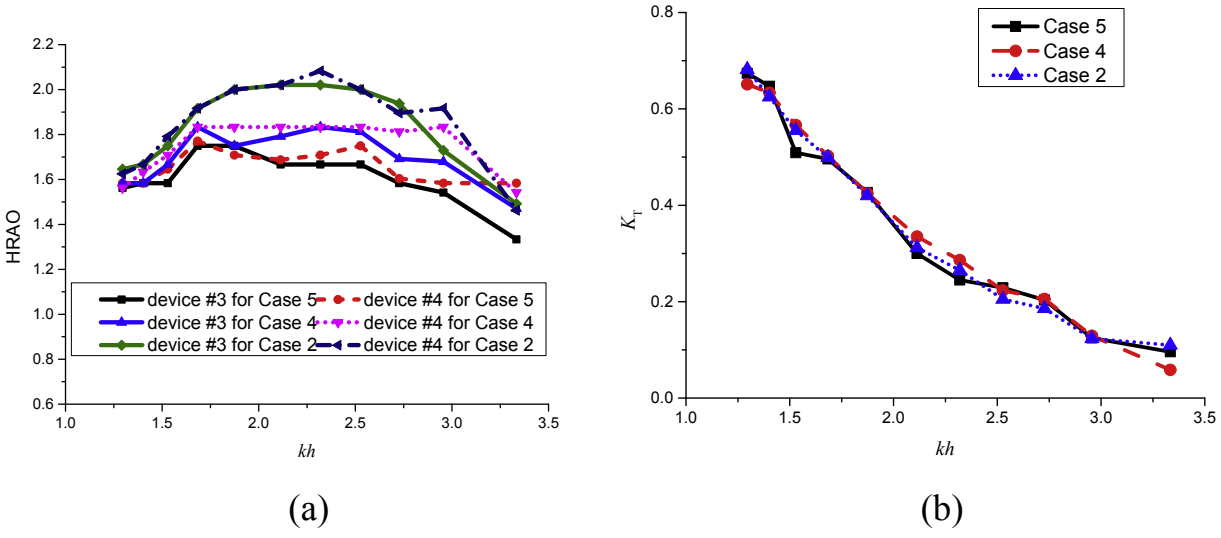

Fig. 10. Variations of the HRAO (a) and transmission coefficient (b) with the dimensionless wavenumber.

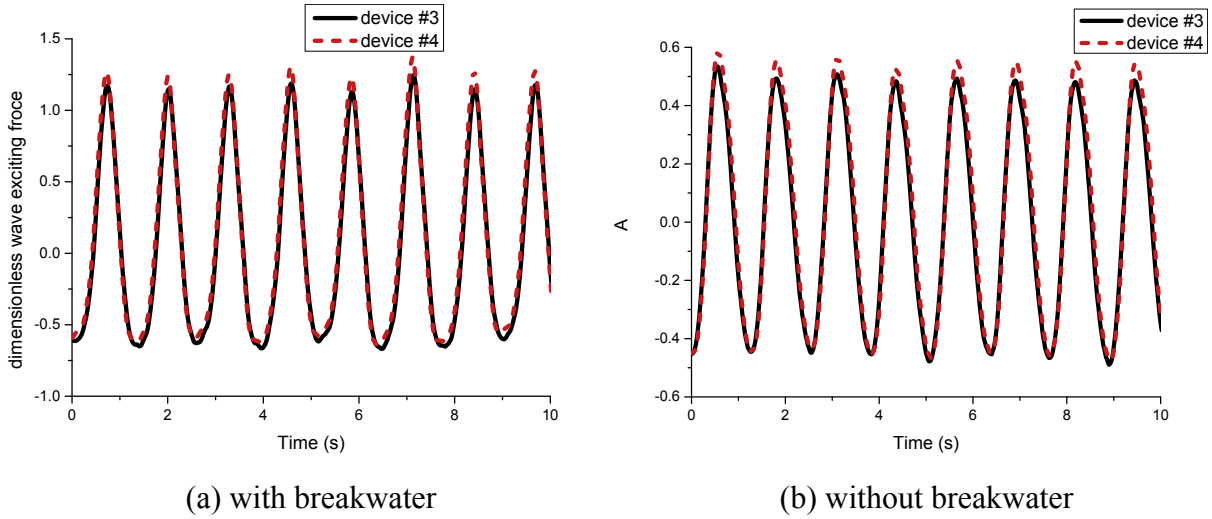

Fig. 11. Time histories of the heaving wave force on the WEC devices (device #3 and device #4) for cases with and without the breakwater (T = 1.27 s, A = 0.06 m, d = 0.20 m, s_1 = 0.05 m).

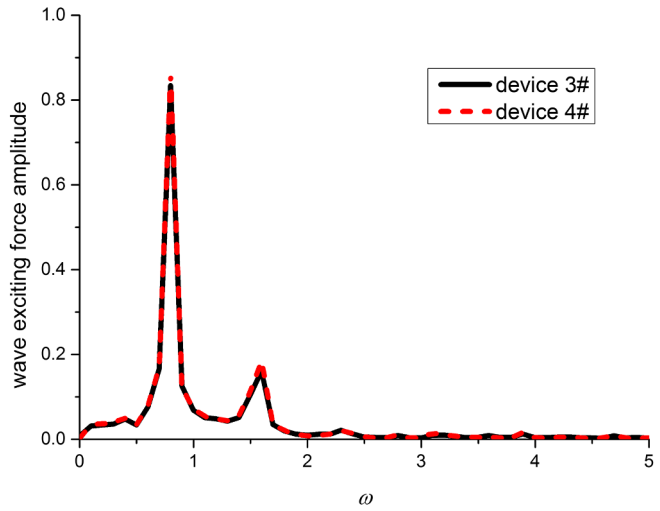

Fig. 12. Amplitude spectral of wave force on the WEC devices with the presence of the pontoon (T = 1.27 s, A = 0.06 m, d = 0.20 m, s_1 = 0.05 m).

lee side of the WEC array. The structure parameters of the circular cylinder and the pontoon in the numerical calculation can be found in section 3.1. The parameters of s_1 and s_2 are 0.05 m and 0.5 m, respectively.

Firstly, to illustrate the role of the external damping on the performance of the WEC array, comparisons of the Capture Width Ratio (CWR) for cases with and without the external PTO damping are made. CWR is often used to balance the PTO performance of a WEC device and defined as the ratio of the generated power and the incident wave power per unit width of the device. The term of external damping b_{ext} is removed from the motion equation while the external damping are considered. The PTO damping λ_c is expressed as

$$\lambda_c = \sqrt{(K/\omega - \omega(M+\mu))^2 + (\lambda + b_{ext})^2} \tag{2}$$

Since the HRAO of the central device in an array with 31 identical devices is in accordance with devices in a channel (see Fig. 5), we evaluate the role of the external damping on performance of the devices in a channel by considering the central device in the array. The size of the devices and the distances between two neighbouring devices are the same as those in the experiment. Fig. 14 shows the variations of CWR of

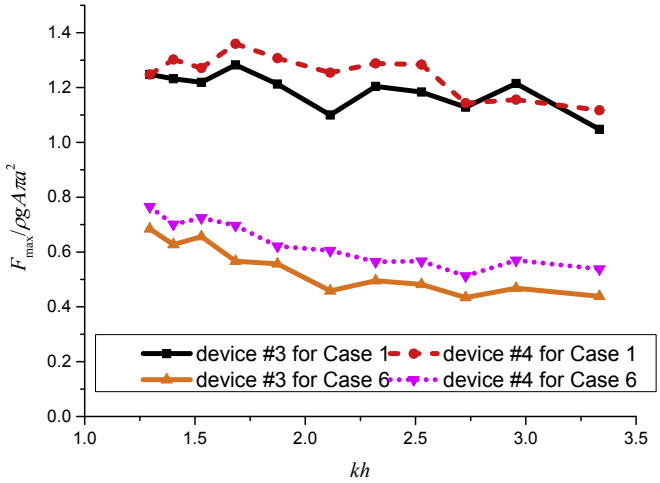

Fig. 13. Variations of F_{max} on the WEC devices with the dimensionless wavenumber kh for cases with and without the pontoon.

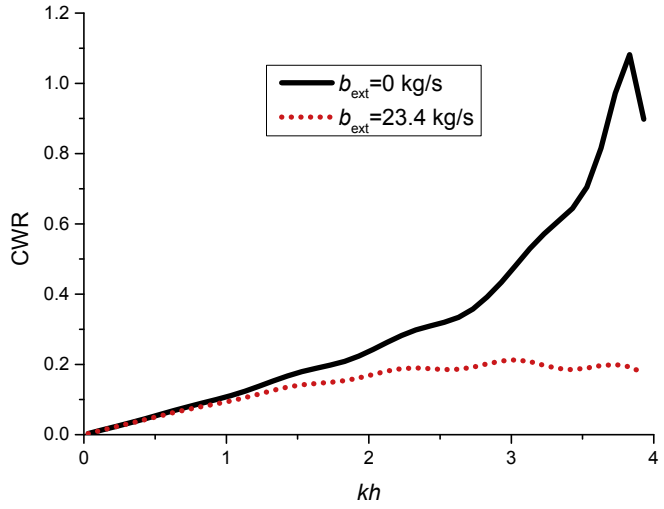

Fig. 14. Variations of CWR of the wave energy device with the dimensionless wavenumber kh.

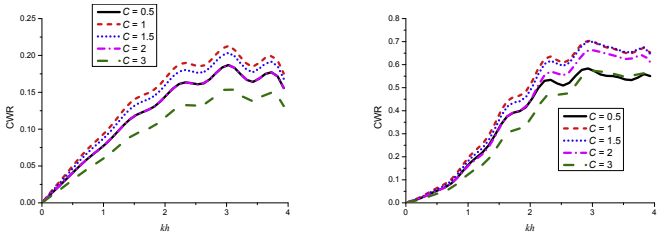

(a) Without pontoon (b) with pontoon

Fig. 15. Variations of CWR on the WEC array with the dimensionless wavenumber *kh* for cases with (a) and without the pontoon (b).

the device at the central location with the dimensionless wavenumber *kh*. From the figure, it can be seen that the external damping mitigates the energy conversion efficiency significantly, especially for the higher frequencies near to the resonance.

To evaluate the effect of the breakwater on the performance of the WEC array (with external damping), the CWR of the WEC array with and without the breakwater are calculated. The draft and width (parallel to the incident waves) of the pontoon in the numerical calculation are the same as those of the pontoon in the experiment. Several PTO damping are chosen by considering $C = 0.1$, 1, 1.5, 2, and 3, where $\lambda_{PTO} = C \cdot \lambda_c$. From Fig. 15, it can be seen that, within the calculated cases, the CWR of the pontoon-integrated WEC array is obviously greater than that without the pontoon. The efficiency of 60% or more can be achieved by properly considering the PTO damping for the system with the pontoon.

4. Conclusions

This paper proposed a breakwater-WEC system, in which an array of OB-WECs are arranged on the weather side of a pontoon-type breakwater. The performance of the conventional WECs and the breakwater-integrated WECs are compared by experimentally investigating the HRAO and wave forces on the WEC devices with and without the breakwater. The experiment design is verifies by comparing with the numerical predictions in terms of the HRAO of the WEC devices. Parametric studies are conducted to investigate the influences of the draft of the WEC devices and pontoon-WEC spacing on the hydrodynamic performance of the breakwater-WEC system. In addition, the effect of the WEC devices on the transmission coefficient of the breakwater system is also considered. As an extension, numerical calculations based on linear potential theory are made to evaluate the performance of the WEC array with and without the breakwater by involving the external damping. The following conclusions have been obtained:

(1) Good agreement of the numerical predictions based on the linear potential flow theory and the experimental data of HRAO can be found by considering the external damping of the floating system.
(2) Compared with the isolated WEC devices, the WEC devices placed in front of a breakwater observe the larger HRAO and wave force (in heave mode), which is beneficial to the efficiency improvement of the WECs.
(3) The HRAO of the WEC devices is sensitive to the draft of the WEC devices and the pontoon-WEC spacing. Within the test cases, the HRAO increases with the decreasing pontoon-WEC spacing, and increases with the increasing draft of the WEC devices.
(4) Even through the external damping mitigates the efficiency of the WEC significantly, useful efficiency (20% approximately) can be achieved for the present integrated system and, at the same time, the CWR of the WEC with the pontoon is obviously greater than that without the pontoon. That's to say, the existence of the breakwater amplifies the energy conversion performance of the WEC array.

Acknowledgement

The authors would like to acknowledge the financial support of the National Natural Science Foundation of China (Grant Nos. 51679036 and 51761135011) and the Royal Academy of Engineering under the UK-China Industry Academia Partnership Programme (Grant No.UK-CIAPP\73).

References

Babarit, A., Clément, A.H., 2006. Optimal latching control of a wave energy device in regular and irregular waves. Appl. Ocean Res. 28, 77–91.
Bellew, S., 2011. Investigation of the Response of Groups of Wave Energy Devices. Ph. D Thesis. University of Manchester.
Boccotti, P., 2007. Caisson breakwaters embodying an OWC with a small opening—Part I: Theory. Ocean. Eng. 34, 806–819.
Chen, W.C., Dolguntseva, I., Savin, A., Zhang, Y.L., Li, W., Svensson, O., Leijon, M., 2017. Numerical modelling of a point-absorbing wave energy converter in irregular and extreme waves. Appl. Ocean Res. 63, 90–105.
Contestabile, P., Iuppa, C., Di Lauro, E., Cavallaro, L., Andersen, T.L., Vicinanza, D., 2017. Wave loadings acting on innovative rubble mound breakwater for overtopping wave energy conversion. Coast. Eng. 122, 60–74.
Drimer, N., Agnon, Y., Stiassnie, M., 1992. A simplified analytical model for a floating breakwater in water of finite depth. Appl. Ocean Res. 14, 33–41.
Falnes, J., Hals, J., 2012. Heaving buoys, point absorbers and arrays. Philos. Trans. R. Soc. Ser. A. 370, 246.
Göteman, M., 2017. Wave energy parks with point-absorbers of different dimensions. J. Fluid Struct. 74, 142–157.
Gomes, R.P.F., Henriques, J.C.C., Gato, L.M.C., Falcão, A.F.O., 2016. Wave power extraction of a heaving floating oscillating water column in a wave channel. Renew. Energy 99, 1262–1275.
Hales, L.Z., 1981. Floating Breakwaters: State-of-the-art Literature Review. Coastal Engineering Research Centre, Fort Belvoir Technical Report No. 81-1.
Howe, D., Nader, J., 2017. OWC WEC integrated within a breakwater versus isolated: experimental and numerical theoretical study. Int. J. Mar. Energ. 20, 165–182.
Journée, J.M.J., Massie, W.W., 2001. Offshore Hydromechanics. Lecture Note. Delft University of Technology.
Karimirad, M., 2014. Offshore Energy Structures: for Wind Power, Wave Energy and Hybrid Marine Platforms. Springer.
McIver, P., Evans, D.V., 1988. An approximate theory for the performance of a number of wave-energy devices set into a reflecting wall. Appl. Ocean Res. 10, 58–65.
Mustapa, M.A., Yaakob, O.B., Ahmed, Y.M., Rheem, C., Koh, K.K., Adnan, F.A., 2017. Wave energy device and breakwater integration: a review. Renew. Sustain. Energy Rev. 77, 43–58.
Mavrakos, S.A., Katsaounis, G.M., Nielsen, K., Lemonis, G., 2004. Numerical performance investigation of an array of heaving wave power converters in front of a vertical breakwater. In: Proceedings of the International Offshore and Polar Engineering Conference, pp. 238–245.
McCartney, B.L., 1985. Floating breakwater design. J. Waterw. Port, Coast. Ocean Eng. 111, 304–318.
Ning, D.Z., Zhao, X.L., Göteman, M., Kang, H.G., 2016. Hydrodynamic performance of a pile-restrained WEC-type floating breakwater: an experimental study. Renew. Energy 95, 531–541.
Ning, D.Z., Zhao, X.L., Chen, F.L., Zhao, M., 2018. Hydrodynamic performance of an array of wave energy converters integrated with a pontoon-type breakwater. Energies 11.
Pecher, A., Kofoed, J.P., 2017. Handbook of Ocean Wave Energy. Springer International Publishing.
Rahmati, M.T., Aggidis, G.A., 2016. Numerical and experimental analysis of the power output of a point absorber wave energy converter in irregular waves. Ocean Eng. 111, 483–492.
Schay, J., Bhattacharjee, J., Soares, C., 2013. Numerical modelling of a heaving point absorber in front of a vertical wall. In: 32nd International Conference on Ocean, Offshore and Arctic Engineering, (pp. V008T09A097).
Tampier, G., Grueter, L., 2017. Hydrodynamic analysis of a heaving wave energy converter. Int. J. Mar. Energ. 19, 304–318.
Teng, B., Taylor, R.E., 1995. New higher-order boundary element methods for wave diffraction/radiation. Appl. Ocean Res. 17 (2), 71–77.
Zhao, X.L., Ning, D.Z., Zhang, C.W., Liu, Y.Y., Kang, H.G., 2017. Analytical study on an oscillating buoy wave energy converter integrated into a fixed box-type breakwater. Math. Probl Eng. 2017 (9).